From Fresnel Diffraction Model to Fine-grained Human Respiration Sensing with Commodity Wi-Fi Devices

Article *in* Proceedings of the ACM on Interactive Mobile Wearable and Ubiquitous Technologies · March 2018

DOI: 10.1145/3191785

CITATIONS
176

READS
1,286

7 authors, including:

Fusang Zhang
Institute of Software, Chinese Academy of Sciences
78 PUBLICATIONS **1,603** CITATIONS
SEE PROFILE

Hao Wang
Boston College
15 PUBLICATIONS **2,077** CITATIONS
SEE PROFILE

Niu Kai
Peking University
35 PUBLICATIONS **1,264** CITATIONS
SEE PROFILE

Beihong Jin
Institute of Software, Chinese Academy of Sciences
198 PUBLICATIONS **1,806** CITATIONS
SEE PROFILE

From Fresnel Diffraction Model to Fine-grained Human Respiration Sensing with Commodity Wi-Fi Devices

FUSANG ZHANG, Peking University; Institute of Software, Chinese Academy of Sciences, China
DAQING ZHANG, Peking University, China
JIE XIONG, University of Massachusetts, Amherst, USA
HAO WANG and KAI NIU, Peking University, China
BEIHONG JIN, Institute of Software, Chinese Academy of Sciences, China
YUXIANG WANG, Peking University, China

Non-intrusive respiration sensing without any device attached to the target plays a particular important role in our everyday lives. However, existing solutions either require dedicated hardware or employ special-purpose signals which are not cost-effective, significantly limiting their real-life applications. Also very few work concerns about the theory behind and can explain the large performance variations in different scenarios. In this paper, we employ the cheap commodity Wi-Fi hardware already ubiquitously deployed around us for respiration sensing. For the first time, we utilize the Fresnel diffraction model to accurately quantify the relationship between the diffraction gain and human target's subtle chest displacement and thus successfully turn the previously considered "destructive" obstruction diffraction in the First Fresnel Zone (FFZ) into beneficial sensing capability. By not just considering the chest displacement at the frontside as the existing solutions, but also the subtle displacement at the backside, we achieve surprisingly matching results with respect to the theoretical plots and become the first to clearly explain the theory behind the performance distinction between lying and sitting for respiration sensing. With two cheap commodity Wi-Fi cards each equipped with just one antenna, we are able to achieve higher than 98% accuracy of respiration rate monitoring at more than 60% of the locations in the FFZ. Furthermore, we are able to present the detail heatmap of the sensing capability at each location inside the FFZ to guide the respiration sensing so users clearly know where are the good positions for respiration monitoring and if located at a bad position, how to move just slightly to reach a good position.

CCS Concepts: • **Human-centered computing** → **Ubiquitous and mobile computing systems and tools**;

Additional Key Words and Phrases: Wireless sensing, Fresnel diffraction model, Human respiration sensing, Wi-Fi

Authors' addresses: F. Zhang, Key Laboratory of High Confidence Software Technologies (Ministry of Education), School of Electronics Engineering and Computer Science, Peking University; State Key Laboratory of Computer Sciences, Institute of Software, Chinese Academy of Sciences, Beijing, China; E-mail: zhangfusang@otcaix.iscas.ac.cn. D. Zhang, Key Laboratory of High Confidence Software Technologies (Ministry of Education), School of Electronics Engineering and Computer Science, Peking University, Beijing, China; E-mail:dqzhang@sei.pku.edu.cn. J. Xiong, College of Information and Computer Sciences, University of Massachusetts, Amherst, USA; E-mail: jxiong@cs.umass.edu. H. Wang and K. Niu, Key Laboratory of High Confidence Software Technologies (Ministry of Education), School of Electronics Engineering and Computer Science, Peking University, Beijing, China; E-mail:China7@pku.edu.cn, xjtunk@pku.edu.cn. B. Jin, State Key Laboratory of Computer Sciences, Institute of Software, Chinese Academy of Sciences, Beijing, China; E-mail:Beihong@iscas.ac.cn. Y. Wang, Key Laboratory of High Confidence Software Technologies (Ministry of Education), School of Electronics Engineering and Computer Science, Peking University, Beijing, China; E-mail:yuxiang.wang@pku.edu.cn. Corresponding Author: Daqing Zhang; E-mail:dqzhang@sei.pku.edu.cn.

2474-9567/2018/3-ART1 $15.00
https://doi.org/0000001.0000001

ACM Reference Format:
Fusang Zhang, Daqing Zhang, Jie Xiong, Hao Wang, Kai Niu, Beihong Jin, and Yuxiang Wang. 2018. From Fresnel Diffraction Model to Fine-grained Human Respiration Sensing with Commodity Wi-Fi Devices. *Proc. ACM Interact. Mob. Wearable Ubiquitous Technol.* 1, 1, Article 1 (March 2018), 23 pages. https://doi.org/0000001.0000001

1 INTRODUCTION

Respiratory rate is an important vital sign, which are used not only to monitor the progression of illness and decline in health, but also to predict emergencies that require immediate clinical attentions such as cardiac arrest [29]. In developed countries, around 5% of the total population suffers from respiration-related illnesses such as Sleep Apnea Syndrome (SAS) and about 30% of people in their seventies are reported to have at least one respiration-related disease [20]. A recent study also shows that disordered breathing is a major cause of Sudden Infant Death Syndrome (SIDS) for sleeping infants and can also lead to abnormal pregnancy outcomes [7] for women who did not have sleep apnea prior to pregnancy. In many instances, patients with respiratory disease only show the symptoms for a short period or at random occasions. Hence, continuous and cost-effective respiration monitoring at home environment is essential.

Two prevailing methods for continuous respiration monitoring in clinical setting are thoracic impedance pneumography [21] and capnography [4]. However, they are not only expensive and intrusive, but also need well-trained caregivers to operate and monitor the devices, which prevent these systems from large scale deployment at ordinary homes. Compared to these invasive respiration sensing methods, contact-free sensing method is more appealing because it neither confines the target with cables or bed, nor causes discomfort or skin irritation from contact with electrodes, straps or devices [33]. Therefore, a lot of research efforts have been devoted to contact-free human respiration rate monitoring. In recent years, RF signals have been employed for localization [14][39], activity tracking [31][40] and even fine-grained gesture recognition [13][36]. However, these systems either employ expensive dedicated hardware such as USRP [34] or require special-purpose FMCW [2][47] and UWB [35] signals which are not available at commodity home devices, significantly limiting their real-life applications. Furthermore, most systems are based on feature training which apply techniques such as SVM, decision tree and CNN for classification and identification. Training based methods need to collect a large amount of activity data samples and are usually sensitive to environmental changes and target variations [43].

The compelling need for a non-intrusive and cost-effective vital sign monitoring system has led researchers to exploit the cheap Commercial Off-The-Shelf (COTS) Wi-Fi devices already widely available at home environment for human respiration sensing. Multiple attempts have shown the feasibility of sensing human respiration rate using commodity Wi-Fi devices [1][17][16][42][18]. However, they failed to answer the most important question: at what locations the subtle respiration is detectable and why other locations are not detectable. There is no theory provided to guide the system design and the researchers have to resort to trial-and-error methods to make the system work. The closest related work was proposed by Wang et al. [9], in which they introduced the Fresnel zone model for respiration sensing. They employ the reflection theory to guide the respiration sensing outside the First Fresnel Zone. However, human respiration sensing in the First Fresnel Zone remains a mystery for researchers. Compared to reflection outside the First Fresnel Zone, more complex diffraction dominates inside the First Fresnel Zone, calling for a theoretical study and systematic solution.

In this paper, we study the respiration detectability inside the First Fresnel Zone with cheap commodity Wi-Fi devices. The Fresnel zone concept originates from Augustin Fresnel's early 19th-century research on light's interference and diffraction [46]. Later the Fresnel Zone model was employed to facilitate wireless communication [5][41]. In the First Fresnel Zone, the recommended obstruction is less than 20%

to make sure most of the energy can be delivered to the receiver and more obstruction inside this zone is considered destructive [6]. In this paper, we turn this "destructive" obstruction in communication into beneficial sensing capability by carefully monitoring the signal variations caused by the diffraction due to human obstruction. For the first time, we apply the diffraction theory inside the First Fresnel Zone (FFZ) to obtain the amplitude variation of the diffracted signal at the receiver and relate the phase change to signal propagation path change and finally to the chest displacement of the human target for fine-grained respiration sensing. We believe this work opens a new direction of applying radio propagation theory to deeply understand and facilitate fine-grained passive sensing.

Furthermore, we model human respiration by considering not only the frontside displacement but also the backside displacement. With the proposed model, we observe surprisingly matching results between theoretical plots and our experimental results, outperforming other state-of-art systems. With the proposed model, we are able to clearly explain why lying generally presents better respiration sensing capability than sitting and how to adjust the device or target position slightly to achieve the best respiration sensing performance. With one pair of Wi-Fi transceivers, each equipped with only one antenna, we are able to monitor the respiration rate at an accuracy higher than 98% at more than 60% of the locations inside the FFZ. Our system is also able to present the detail heatmap indicating where are the good and where are the bad positions for respiration sensing for all the locations inside FFZ. Our method can be easily extended to many other applications which require fine-grained movement tracking such as hand/finger gesture recognition and coarse-grained human activity sensing such as workout monitoring. The main contributions of this paper include:

- This is the first work applying the Fresnel diffraction model for human respiration monitoring and analysis within the FFZ. This work provides a general theoretical foundation for fine-grained human and object movement sensing in indoor environment.
- By analyzing how a moving object within the FFZ affects the received RF signal and modeling a human target as a varying-size cylinder, we develop the mathematical model to relate one's location to the detectability of respiration within the FFZ. We revealed multiple unique properties for respiration sensing inside the FFZ: 1) While the chest frontside movement dominates, the backside movement does affect the sensing capability; 2) A good respiration sensing position for person A may not be a good position for person B due to body thickness difference; 3) While the positions at line of sight (LoS) are good for lying scenario respiration sensing, they are bad for sitting.
- We implemented the system with cheap commodity Intel 5300 Wi-Fi cards and verified the proposed mathematical model with comprehensive experiments. At more than 60% positions inside the FFZ when the target is lying, the accuracies of respiration rate monitoring are higher than 98%.

2 UNDERSTANDING FRESNEL DIFFRACTION MODEL

In this section, we first introduce the basics of the Fresnel diffraction model in free space. When the target is located within the FFZ, diffraction is much stronger than reflection and thus diffraction dominates [22]. To understand the diffraction in the FFZ, we illustrate the concept with a single point target first. Then, we generalize the target to a rectangular plate and a circular cylinder to understand the diffraction effect on the received RF signal at the receiver.

2.1 The basics of the Fresnel Diffraction model

We pay attention to the First Fresnel Zone because more than 70% of the energy is transferred via this zone [11]. When a target moves in this zone, the amplitude and phase of the received signal can be greatly affected. Consider a free space scenario, two transceivers T and R transmit RF signals with a wavelength

of λ. The Fresnel zones are concentric ellipses as shown in Fig. 1. The middle point of two transceivers is denoted as O, the length of TO and RO are d_1 and d_2 [1], respectively. Now we pick a point Q in the FFZ. Without loss of generality, we assume QT equals to QR for easier illustration. We denote the vertical distance from Q to O as h. The signal propagates from this point Q has a diffraction effect at the receiver side. We present the detailed derivative process in detail as follows [22].

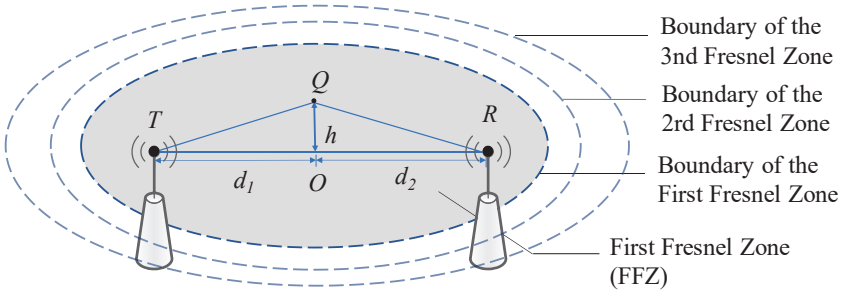

Fig. 1. Geometry of the Fresnel Diffraction at point Q.

We first calculate the path differences Δd between TQR and TOR

$$\begin{aligned}\Delta d &= |TQR| - |TOR| \\ &= \sqrt{(d_1)^2 + (h^2)} + \sqrt{(d_2)^2 + (h^2)} - (d_1 + d_2) \\ &= d_1\sqrt{1 + (h/d_1)^2} + d_2\sqrt{1 + (h/d_2)^2} - (d_1 + d_2)\end{aligned} \tag{1}$$

For FFZ, $h \ll d_1$ and $h \ll d_2$, thus $(h/d_1)^2 \ll 1$ and $(h/d_2)^2 \ll 1$. By employing the approximation $\sqrt{1+x} \approx 1 + \frac{x}{2}$ when $x \ll 1$, Eq. 1 can be simplified as

$$\Delta d \approx \frac{h^2}{2}\frac{(d_1 + d_2)}{d_1 d_2} \tag{2}$$

In context of signal propagation, the corresponding phase difference caused by this path difference Δd is

$$\varphi = \frac{2\pi\Delta d}{\lambda} = \pi h^2 \frac{(d_1 + d_2)}{\lambda d_1 d_2} \tag{3}$$

The Fresnel-Kirchhoff diffraction parameter v is defined as

$$v = h\sqrt{\frac{2(d_1 + d_2)}{\lambda d_1 d_2}} \tag{4}$$

Thus, the phase difference can be simplified as $\varphi = \frac{\pi}{2}v^2$, and this additional phase change occurs at the diffracted signal through Q compared to the direct path signal from T to R.

2.2 How a moving target affects the RF signal?

In reality, the target has a nonnegligible size. We first analyze how the signal gets changed when a metal plate moves across the FFZ. To study the diffraction effect at only one edge of the plate, we assume the

[1]Note that when O is the middle point, $d_1 = d_2$

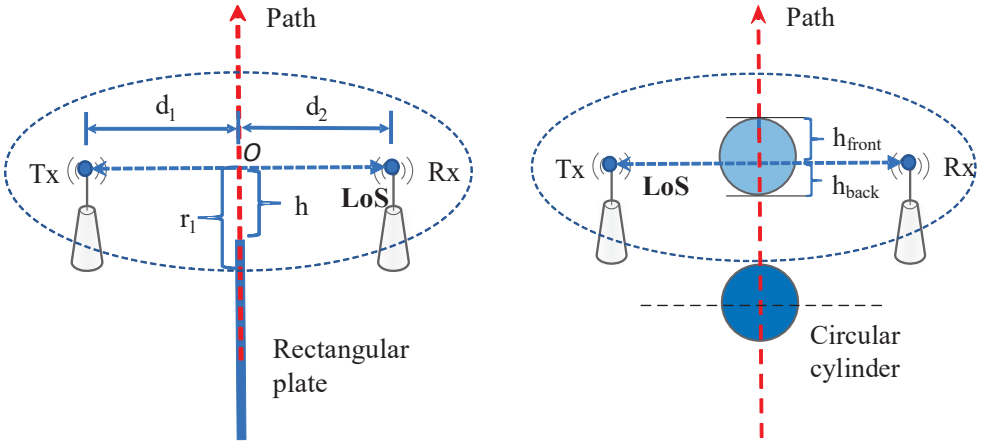

(a) Rectangular plate case (b) Circular cylinder case

Fig. 2. Rectangular plate and circular cylinder move across the FFZ.

metal plate has an infinite length and only one side moves across. The radius r_1 of the FFZ as shown in Fig. 2 is

$$r_1 = \sqrt{\frac{\lambda d_1 d_2}{d_1 + d_2}} \tag{5}$$

We further define a parameter u called **Fresnel clearance** to indicate the percentage of crossing

$$u = \frac{h}{r_1} \tag{6}$$

where h is the vector distance from O to the edge of the metal plate. When the plate edge just touches the line of sight (LoS) of the two transceivers, $h = 0$. When the plate edge first touches the boundary of the FFZ, $h = -r_1$. When the plate reaches the other side of the boundary, $h = r_1$. So u is in the range of -1 to 1. Based on this definition, the Fresnel-Kirchho diffraction parameter v can be expressed by Fresnel clearance u as

$$v = h\sqrt{\frac{2(d_1 + d_2)}{\lambda d_1 d_2}} = h\frac{\sqrt{2}}{r_1} = \sqrt{2}u \tag{7}$$

Thus, the signal amplitude at the receiver end due to diffraction can be expressed as [22]

$$F(v) = \frac{1+j}{2} \cdot \int_v^{\infty} exp(\frac{-j\pi z^2}{2})dz \tag{8}$$

and $F(v)$ is known as Fresnel integral. The diffraction gain due to the presence of the metal plate is given by

$$Gain_{Diff} = 20log|F(v)| \tag{9}$$

In reality, the human target has a finite size. When a person is present in the FFZ, the signals have diffractions at both sides of the human body. Thus, we next study the diffraction effect of a circular

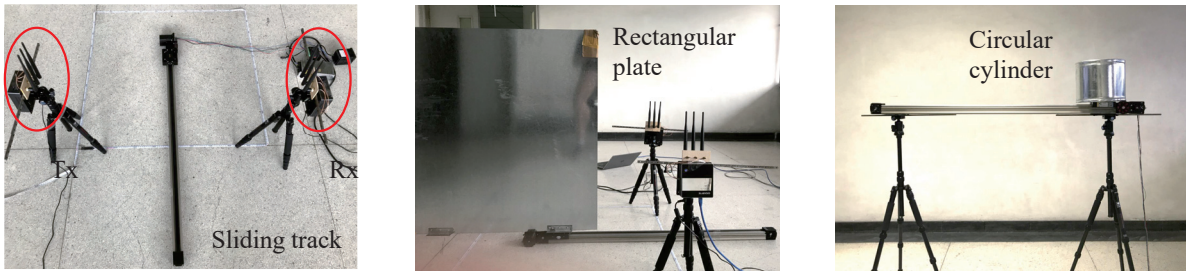

Fig. 3. Deployment of transceivers and two experimental scenarios.

cylinder with a limited size (e.g., a diameter of 12 cm) when it crosses over the FFZ. The cylinder moves along the perpendicular bisector of the two transceivers as shown in Fig. 2b.

We now define two new parameters **Fresnel front clearance** u_{front} and **Fresnel back clearance** u_{back}. The diffraction effect of the circular cylinder consists of two parts, i.e., the diffraction caused by the front side and by the back side. The Fresnel front clearance $u_{front} = \frac{h_{front}}{r_1}$ reflects the relative position of the front side of the target inside the FFZ. h_{front} is the distance from the front side of circular cylinder to the LoS of the two transceivers. So the Fresnel front integral is given as

$$F(v_{front}) = \frac{1+j}{2} \cdot \int_{v_{front}}^{\infty} exp(\frac{-j\pi z^2}{2})dz \tag{10}$$

Similarly, the Fresnel back integral is given as

$$F(v_{back}) = \frac{1+j}{2} \cdot \int_{-\infty}^{v_{back}} exp(\frac{-j\pi z^2}{2})dz \tag{11}$$

The overall diffraction gain due to the presence of a limited size circular cylinder is thus given by

$$Gain_{Diff} = 20log|F(v_{front}) + F(v_{back})| \tag{12}$$

2.3 Verification with benchmark experiments

In this section, we verify the Fresnel diffraction effect with real-life experiments. We consider two different moving subjects, i.e., a large metal plate and a small circular cylinder.

2.3.1 Experimental setup. The two Wi-Fi transceivers are placed 100 cm apart. A sliding track with a length of 150 cm is employed to move the metal plate smoothly into the FFZ as shown in Fig. 3. The metal plate has a size of 100×100 cm. The two circular cylinders used in the experiments have a diameter of 6 cm and 12 cm, respectively while the lengths of the cylinders are both 20 cm. Our system does not need an antenna array. In the experiments, each transceiver is equipped with three antennas but only one is used for transmission/reception. The antennas at the two transceivers are placed at the same height. We adjust the height of the two antennas to be 65 cm and 110 cm above the ground in the experiments. The sliding track is aligned with the perpendicular bisector of the transceivers. The central carrier frequency is 5.24 GHz and the signal wavelength is 5.7 cm.

2.3.2 Benchmark experiments. To verify the diffraction effect in the FFZ, we move the metal plate along the sliding track with the Fresnel clearance parameter u varied from -2 to 2 (i.e., h is varied from

$u \times r_1 = -2 \times \sqrt{\frac{\lambda d_1 d_2}{d_1+d_2}}$=-23.87 to 23.87 cm). Note that the radius of the second and third Fresnel zones are $r_2 = \sqrt{\frac{2\lambda d_1 d_2}{d_1+d_2}}$=16.88 cm and $r_3 = \sqrt{\frac{3\lambda d_1 d_2}{d_1+d_2}}$=20.67 cm, respectively. Thus, moving along the sliding track, the metal plate will first touch the boundary of the 3rd Fresnel Zone and later the boundary of the 2nd Fresnel Zone. Then it reaches the boundary of the FFZ and finally the LoS of the two transceivers. After that, it moves out of the FFZ gradually. With Eq. 9, we obtain the theoretical diffraction gain (i.e. the normalized signal amplitude with respect to the scenario when there is no target) during the whole moving process in Fig. 4a (bottom). Before touching the boundary of the FFZ, we observe one peak and one valley near to the 3rd and 2nd Fresnel Zone boundaries (i.e., at $u = -1.73$ and $u = -1.41$). The peak near to the FFZ boundary appears inside the FFZ at $u = -0.85$. Then the amplitude keeps decreasing until the end.

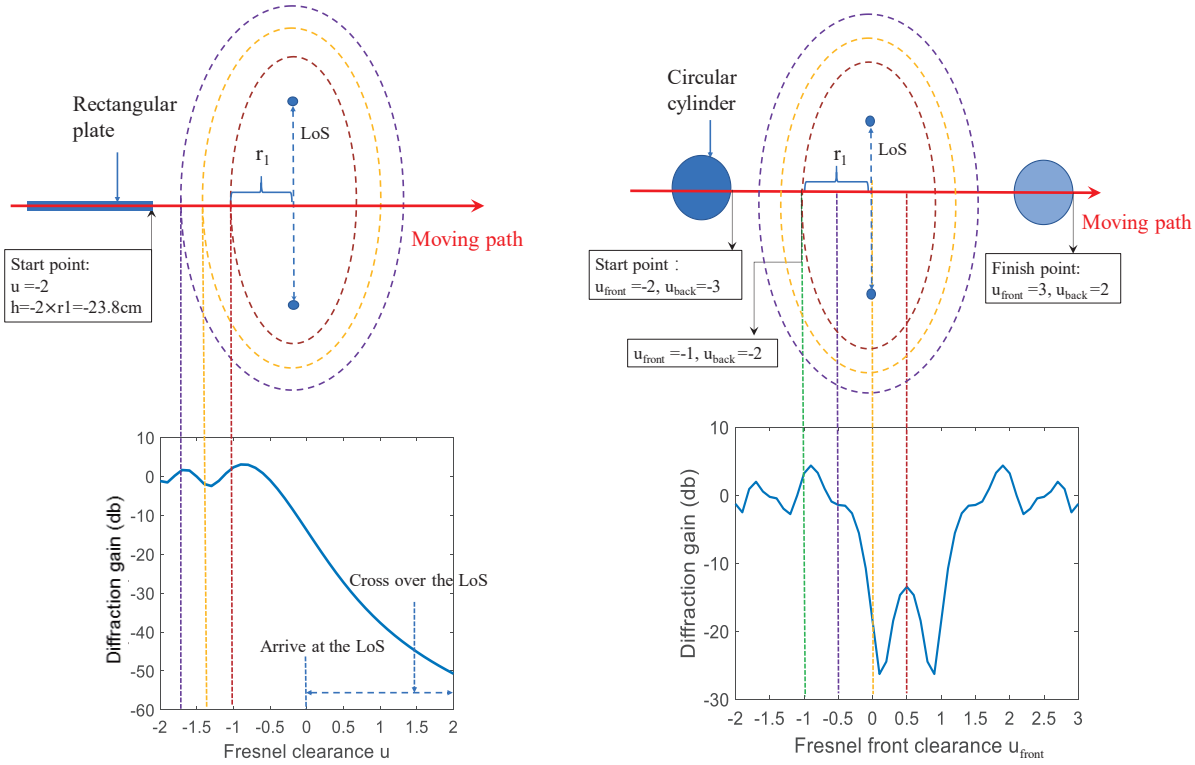

(a) Move the metal plate across the FFZ

(b) Move the cylinder across the FFZ

Fig. 4. The diffraction gain change with targets moving across the FFZ.

Next, we let the circular cylinder with a diameter 12 cm move along the perpendicular bisector of the two transceivers, starting from Fresnel front clearance u_{front} =-2 and stoping at Fresnel front clearance u_{front} =3. By calculating both the Fresnel front and back integrals with Eq. 12, the diffraction gain is plotted in Fig. 4b (bottom). Before the cylinder touches the LoS, the amplitude also experiences a peak and a valley. When the front side of the cylinder moves to the middle point (u_{front} =-0.5) of the first half of the FFZ, the amplitude has a short plateau, then it drops rapidly until the cylinder reaches

the LoS. Interestingly, after the cylinder crosses cover the LoS, the amplitude increases again until the cylinder reaches $u_{front} = 0.5$ (the gravity center of the cylinder is on the LoS). The overall shape exhibits a symmetrical pattern with respect to $u_{front} = 0.5$.

2.3.3 Results analysis. We present the experimental results for the 6 cm cylinder with both commodity Wi-Fi card and software-defined radio WARP platform in Fig. 5. We can see that the experimental results match the theoretical plots very well. Compared with software-defined radio platform, the data obtained from commodity Wi-Fi device is much more noisy so the curve is not as smooth as the one generated with data obtained from WARP. The results for the metal plate and the 12 cm cylinder also match the theoretical plots well and we skip them here.

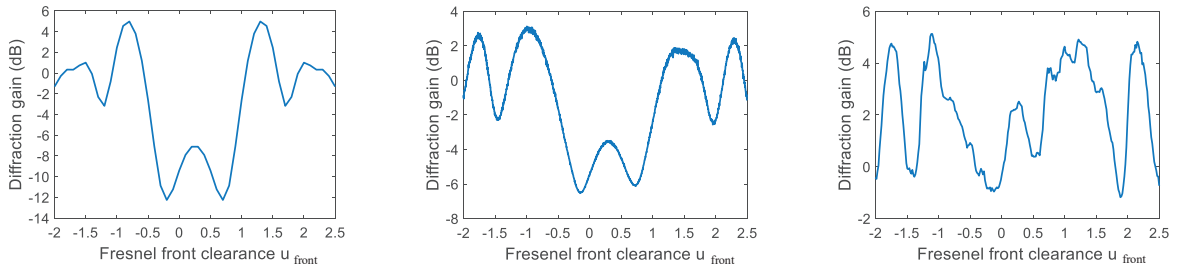

(a) Theoretical results (b) Software-defined radio WARP (c) Commodity Intel 5300 Wi-Fi card

Fig. 5. Diffraction gain variation when a 6 cm diameter cylinder moves across the FFZ

2.4 Key properties revealed from the Fresnel diffraction model

With the above experiments, we summarize the unique diffraction-related properties in the FFZ which can be used for respiration sensing as follows:

(1) The boundary of the FFZ is not necessarily the highest power point. The peak occurs at a position slightly after entering the FFZ. This motivates us to learn that the best and worst sensing positions may not be located on the FFZ boundary.
(2) The object with a small size has double-side diffraction when located inside the FFZ. For the circular cylinder, the diffraction gain during the process of crossing the FFZ is non-monotonous. The local peak at the bottom appears when the gravity center of the cylinder is on the LoS. This property explains why good positions for respiration sensing appear alternatively when the target is sitting in Sec. 3.3.
(3) The objects with different diameters have slightly different diffraction effects, leading to different sizes and positions of the bumps. This presents us a hint that different-size persons may have distinct sensing capabilities at the same position within the FFZ.

3 SENSING HUMAN RESPIRATION IN THE FFZ

In this section, we model the human body for two commonly seen scenarios: (i) lying on the bed and (ii) sitting in the chair. Two different models are proposed for these two scenarios based on the observations in the previous section. We convert the chest displacements to fine-grained signal phase changes to characterize the human respiration process. With a careful study of the sensing capability at each small grid, we are able to present the respiration sensing capability heatmap for both lying and sitting. At the same time, we show the effects of body thickness and respiration depth on respiration sensing.

3.1 Modeling human respiration

According to previous study [19], the chest displacement during respiration is 4.2∼5.4 mm in front dimension, 2.5∼2.6 mm in back dimension, and 0.6∼1.1 mm in mediolateral dimension. During deep inspiration breath hold (DIBH), chest displacement can be increased up to 12.6 mm in anteroposterior dimension. We model human body when lying on the bed and sitting in the chair separately as they are quite different during respiration. Human body is modeled as a varying size flat-cylinder shown in Fig. 6a, where the outer and inner cylinder surfaces correspond to the chest positions for inhalation and exhalation, respectively. Consider a human body lying on the bed between the transceivers in Fig. 6c, the respiration process is similar to that of a metal plate moving in and out with a displacement of around 5 mm. The key difference between a human body and a metal plate is that the human subject has a nonnegligible breadth. Fortunately, the multiple knife-edge diffraction theory [33] addresses the problem and points out that the effect of many obstructions in FFZ is equivalent to the single highest obstruction as shown in Fig 6b. In this way, we can model the human body during respiration in the lying scenario as a plate with a tiny movement in the FFZ.

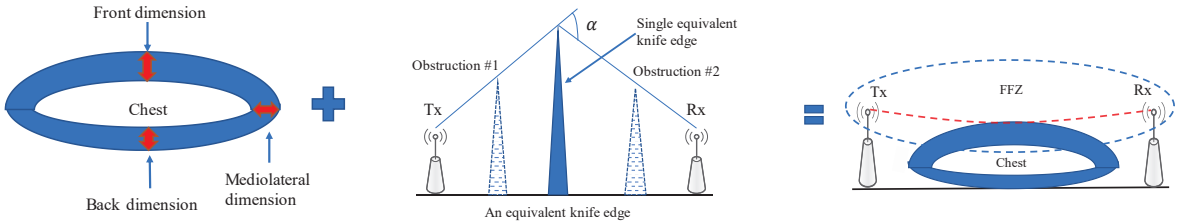

(a) Human modeling (b) Multiple knife-edge diffraction (c) Chest model when lying on the bed

Fig. 6. Model human body lying on the bed

Next, we model human body while sitting in the chair. The chest model is still a varying size cylinder. However, different from lying on the bed, the chest displacements in both front and back dimensions need to be considered now. Inspired by the circular cylinder example in the previous section, we model a sitting or standing human's respiration as a cylinder with a movement of 5 mm in front dimension and 3 mm in back dimension. Diffractions at both sides occur while the subject is sitting in the FFZ as shown in Fig. 7. The Fresnel front and back clearances should both be considered to calculate the diffraction gain for fine-gained respiration sensing.

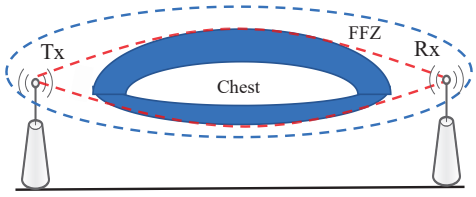

Fig. 7. Model human body sitting in the chair

3.2 Converting chest displacement to phase change

In this section, we study how to extract the phase change caused by chest displacement from the received RF signal. We first convert the chest displacement to the change of the diffraction path length, and then convert this path length change to phase change. Assume the chest displacement is Δd, the path length change caused by the movement is around $2\Delta d$. One wavelength of path change exhibits a phase change of 2π. Hence, the phase rotation θ caused by respiration is calculated as

$$\theta = 2\pi \times \frac{2\Delta d}{\lambda} \tag{13}$$

where λ is the wavelength which is 5.7 cm for 5 GHz signals. For ordinary and deep respiration, the amount of chest displacement Δd is 5 mm and 12 mm, corresponding to a phase change of 60° and 150°, respectively. As shown in Fig. 8, what is really important is that the amplitude variation caused by the respiration is highly dependent on the target position in the FFZ. The same amount of chest displacement causes very different amplitude variations. When the chest displacement occurs in the monotonic interval, the received signal fluctuation due to respiration is larger. On the other hand, in the nonmonotonic interval, the fluctuation is weaker and thus easier to be submerged by noises.

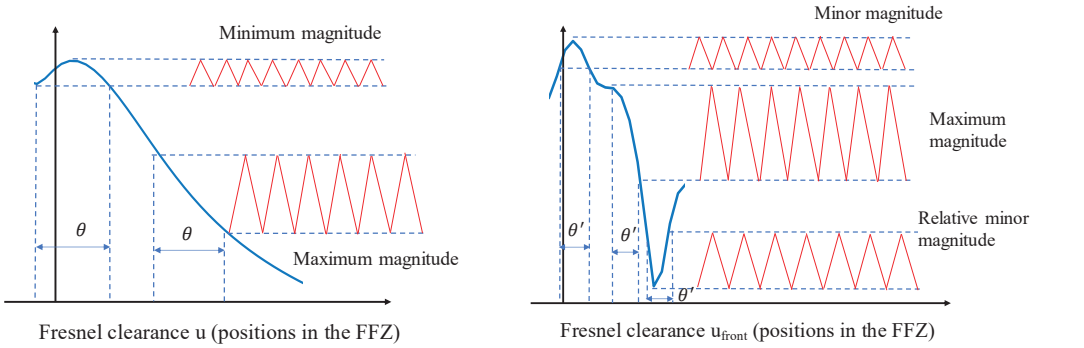

(a) Lying scenario generated wave in FFZ (b) Sitting/standing scenario generated wave in FFZ

Fig. 8. The wave fragmentation under two scenarios.

3.3 Impact of chest location inside the FFZ

Where are the best and worst positions for respiration sensing in the FFZ? We answer this question by studying the lying and sitting/standing postures separately. The distance between the two transceivers is set as 100 cm. The body thickness of the subject is assumed to be 24 cm. Without loss of generality, we let the human subject lie or sit along the perpendicular bisector of the two transceivers. For the lying posture, the chest displacement in front dimension is assumed to be 5 mm. For the sitting/standing posture, the chest displacements in front and back dimension are assumed to be 5 mm and 3 mm, respectively. To investigate the respiration detectability at different positions in the FFZ, we choose three typical Fresnel clearance values $u = -1, -0.5, 0$ for lying and correspondingly $[u_{front}, u_{back}]$ = [-1, -3], [-0.5, -2.5], [0, -2] for sitting/standing. Fig. 9 shows the respiration caused signal amplitude variations for lying. The amplitude variations of signal in Fig. 9a, 9b and 9c are 0.44, 0.88 and 1.2, respectively. We can see that

the boundary of the FFZ ($u = -1$) is not a good position for respiration sensing. When the chest front end moves to the middle of the half ellipse ($u = -0.5$) and further touches the LoS, the detectability is enhanced obviously.

Fig. 10 shows the signal variation in the sitting/standing scenario. Overall the detectability is lower compared to the lying scenario due to diffraction at both sides. The amplitude variations of signal in Fig. 10a, 10b and 10c are 0.11, 0.4 and 0.4, respectively. While the boundary of FFZ is also a bad position, moving inside presents much larger variations and thus much better performance for sensing. Next, we explore the worst position for respiration sensing in the FFZ. As shown in Fig. 4a, the highest point is not on the FFZ boundary ($u = -1$) but appears at $u = -0.85$ for lying. The radius of FFZ is 11.9 cm and thus the worst position is 10.1 cm away from the LoS.

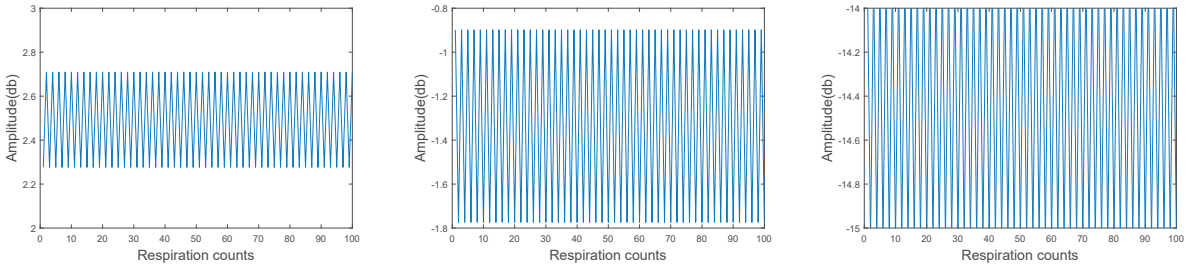

(a) $u = -1$ (b) $u = -0.5$ (c) $u = 0$

Fig. 9. Different Fresnel clearance under lying scenario.

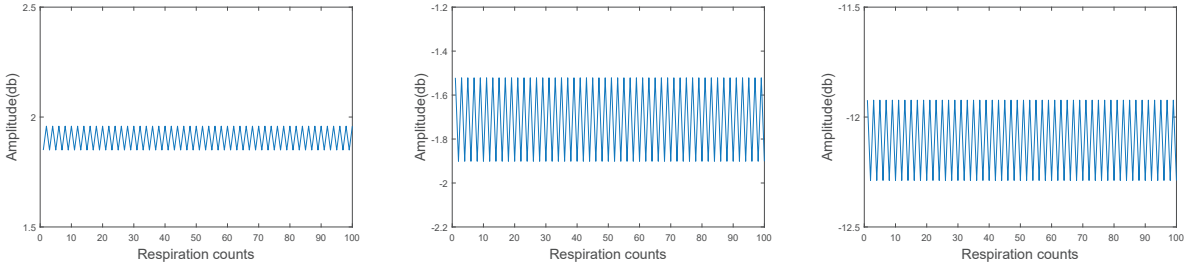

(a) $u_{front} = -1, u_{back}$=-3 (b) $u_{front} = -0.5, u_{back} = -2.5$ (c) $u_{front} = 0, u_{back} = -2$

Fig. 10. Different Fresnel front and back clearance under sitting/standing scenario.

3.4 Impact of body thickness

In this section, we study the impact of human body thickness in respiration sensing. The body thickness of an ordinary person is around 20 cm. We consider two human subjects with thickness of 20 cm and 25 cm for lying scenario. The distance from the subject's back to the LoS is 30 cm. The amplitude variation (0.08) is very small for the target with a 20 cm thickness. However, for the subject with a thickness of 25 cm, the amplitude variation (0.98) is much larger and can be accurately detected. Note that the two subjects have the same u_{back} so the u_{front} is -0.85 for subject A and -0.43 for subject

B, which are quite different. This causes a different diffraction effect and accordingly a very different respiration detectability. Thus, a good position for person A may not be a good position for person B.

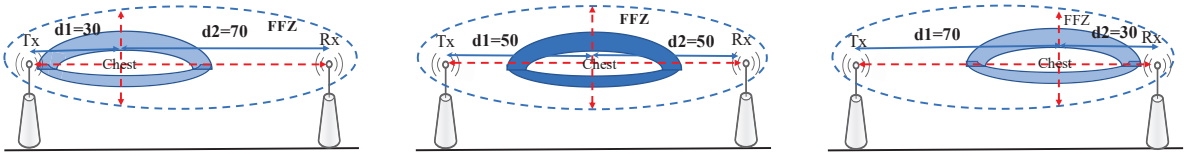

(a) Move to the left (b) At the middle (c) Move to the right

Fig. 11. Different distances to transceivers

3.5 Impact of subject's distance to transceivers

When the sensing capability is low at a position, a natural idea is to move closer to one of the transceivers. In this section, we study the impact of the subject's distance to transceivers, that is, the subject is not on the perpendicular bisector of the transceivers but moves near to one of the transceivers as shown in Fig. 11 (a-c). We consider three scenarios: the person is in the middle (d_1=50 cm, d_2=50 cm), the person moves to the left (d_1=30 cm, d_2=70 cm) and to the right (d_1=70 cm, d_2=30 cm). For a bad position ($u = -0.8$), the amplitude variations of the signals are 0.27, 0.25 and 0.27 respectively for the three scenarios. We find that the sensing capability does not improve much. In principle, at the middle point, the FFZ radius r_1 is $\sqrt{\frac{\lambda \times 50 \times 50}{50+50}}$=11.9 cm. While at the left and right positions, the FFZ radius $r_1^{'}$ is changed to $\sqrt{\frac{\lambda \times 30 \times 70}{30+70}}$ =10.9 cm. This change of radius makes the Fresnel clearance parameter u change from 0.8 to 0.87. So a 20 cm movement only causes a FFZ radius change of 1 cm, and a Fresnel clearance change of 0.07. This demonstrates that moving closer to the transceivers is not an effective way to improve the sensing capability.

4 EVALUATION

To validate the Fresnel diffraction theory for RF-based human respiration sensing, we utilize the off-the-shelf Wi-Fi devices for our experiments. We conduct comprehensive experiments and report the results in this section.

4.1 Experimental setup

The prototype system consists of two Wi-Fi transceivers. Each transceiver is a mini-pc equipped with a cheap Intel 5300 Wi-Fi card. We only use one antenna at each transceiver and the signal is transmitted in the 5.24 GHz frequency band. The two transceivers are placed with a distance of 100 cm between each other at the same height [2]. The packet transmission rate is 20 packets per second. We collect the CSI data from the commodity Wi-Fi card without any filter [8]. Each CSI stream contains readings from 30 subcarriers. Respiration is known to be a periodic motion, thus we extract the respiration rate using the FFT function (argmax(abs(fft(x)))). The output of argmax(abs(fft(x))) corresponds to the dominant frequency, which is the respiration rate of the target. The ground truth of respiration rate is calculated

[2]Note that this height changes with varying Fresnel clearance values.

(a) lying (b) sitting

Fig. 12. Real deployment of lying and sitting for human respiration sensing.

as $\frac{number\ of\ breaths}{recording\ time}$. During the respiration detection process, the subject (target) is asked to count the number of respirations himself/herself. Meanwhile, another person (non-target) separately counts the number of respirations as verifications. Only when the two counts from the target and non-target match, we take the count as the ground-truth. We also employ a fiber-based system (VitalPro 4374 Fiber Sensor Mat) to provide ground truths when the target is lying. We deploy the system as we described in Section 2.3.1. Fig. 12 shows the experimental setup for lying and sitting scenarios, respectively.

4.2 Overall performance

We recruit eight participants including one female and seven male students for evaluation. We ask them to lie on the bed and breathe naturally. We record five sets of monitoring data for each participant including three 1-min, one 2-min and one 5-min at different good positions. We then repeat the process to record five sets of monitoring data at different bad positions. We define the position where the accuracy of respiration rate can reach above 95% as a good position and the position with an accuracy below 70% as a bad position. We build a web-based interface to show the breathing rates along with a real-time video recording.

Fig. 13 shows the acquired average respiration rates of the eight participants and their ground truths. For the good positions, the overall estimation accuracy is as high as 98.8%. For bad positions, the accuracy decreases to 61.5%. For a good position, we can explicitly identify the periodical variations caused by respiration and obtain the respiration rate at a high accuracy. Whereas for a bad position, there are false positive peaks. Fortunately, with our method, we know clearly where those good positions are located in the FFZ and can easily adjust the height of the transceivers or ask the target to move slightly to be located at a good position. Among the eight participants, we observe that one of them (Person 1) breathes much faster and another one (Person 2) breathes much slower than the others.

4.3 Heatmap visualization of good and bad positions

It is very useful to know where are those good positions in the FFZ for respiration sensing. We employ a heatmap to visualize this information at all locations within the FFZ. Note that different subjects with different body thicknesses cause slightly different heatmaps. We generate the heatmap of the respiration

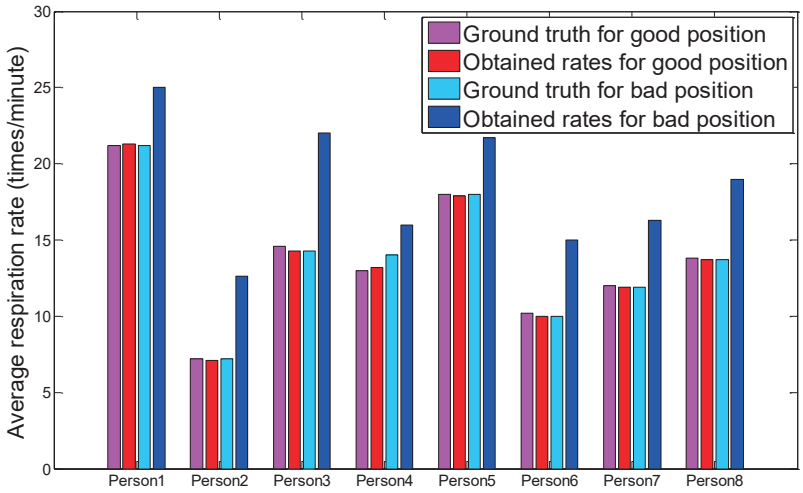

Fig. 13. Respiration rates of different participants

sensing for a subject with a 24 cm body thickness in both lying and sitting scenarios in Fig. 14. For lying, the boundary ($u = -1$) of the FFZ is not a good position. The worst position ($u = -0.85$) is close to the boundary. Going further inside, we obtain good positions until the LoS. Note that for $u > 0$, the sensing capability slightly decreases monotonously but respiration is still detectable before u=1 according to the diffraction gain curve. So it is easy to obtain a good position for lying. Among all the positions inside the FFZ, with the cheap commodity Wi-Fi hardware, we can achieve high monitoring accuracies at around 60% locations. Note that this number can be further increased with more advanced signal processing techniques to remove the hardware noise or employ software-defined radio platform such as WARP and USRP which have significantly less noise. For the sitting scenario as shown in Fig. 14b, the good position and bad position appear alternatively. Moving from the boundary inside and before touching the LoS, there are three locations at Fresnel clearance $u = -0.88, -0.63$ and -0.22, where the respiration sensing

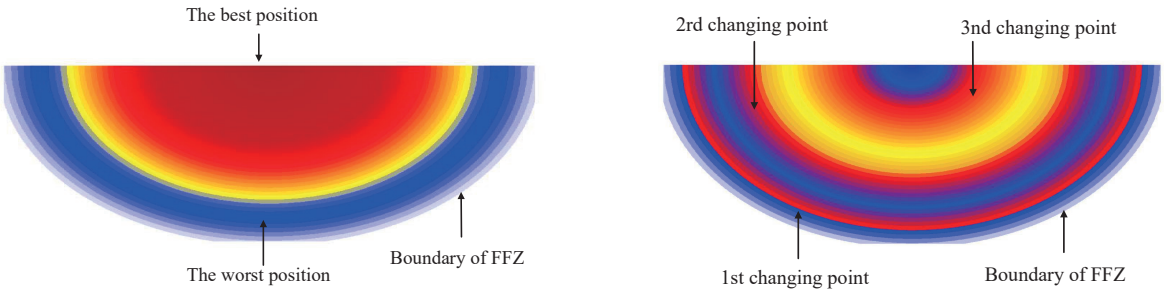

(a) The heat map of lying postures

(b) The heat map of standing/sitting postures

Fig. 14. Heat maps of two scenarios (viewed positions in color).

capability is significantly improved. Among them, $u = -0.22$ is the best position. The boundary of the FFZ and the area close to LoS are both bad positions. The noncontinuous nature of the heatmap indicates that the respiration sensing for sitting scenario is more complicated than lying.

4.4 Impact of subject's position

Now we zoom in to see the detail diffraction gain variations at several typical positions. We ask each subject to lie on the bed and breathe naturally. Each subject is moved to vary the Fresnel clearance parameter u from 0 to -0.85, and finally -1. The results are shown in Fig. 15. We can see that $u = 0$ is a good position. Instead, $u = -0.85$ and $u = -1$ are two bad positions at which the signal variations are much smaller. These results match the theoretical analysis in Section. 3.3 perfectly. From the theoretical analysis, we know that $u = 0$ and $u = -0.85$ are the best and worst positions among all locations in the FFZ.

When a subject sits in a chair, the overall performance is indeed not as good as lying down. Among the three positions, u_{front}=-1 is an undetectable case. The signal variation caused by respiration is too small and submerged in the noise. We can observe clear periodic fluctuations when u_{front}=0. The position u_{front}=-0.85, which is a bad position for lying turns to be a good position for sitting as the diffraction caused by the back displacement increases the overall variation.

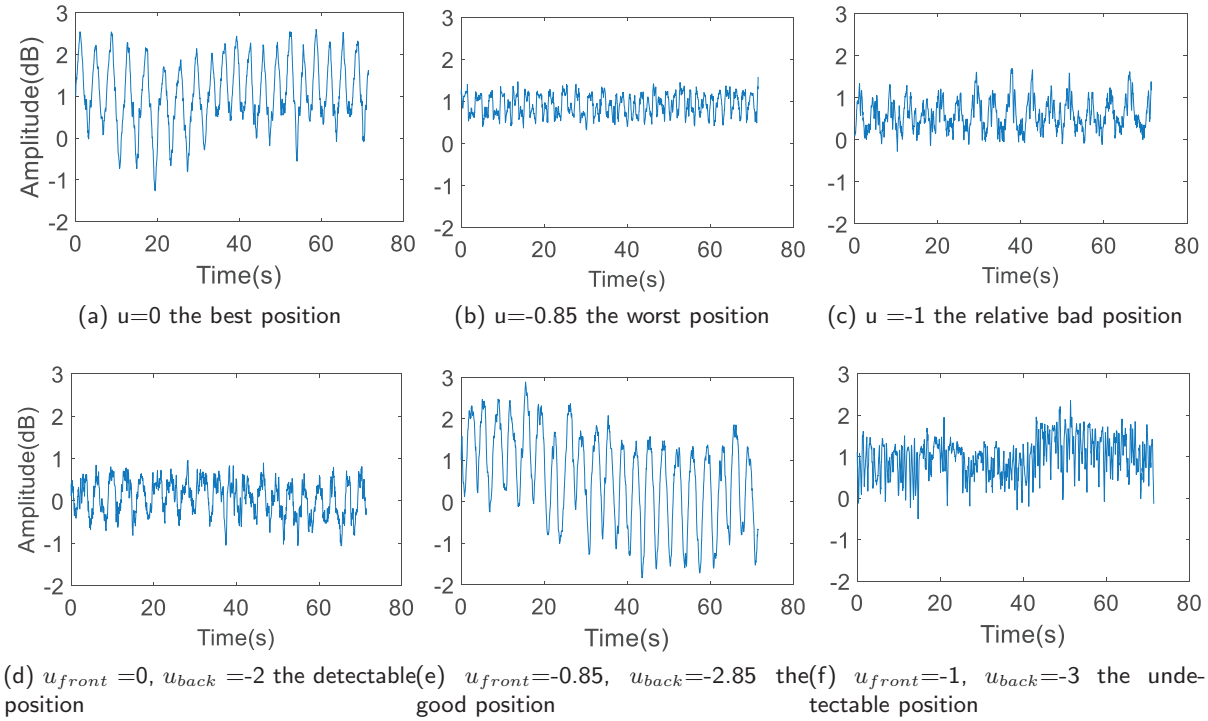

(a) u=0 the best position (b) u=-0.85 the worst position (c) u =-1 the relative bad position

(d) u_{front} =0, u_{back} =-2 the detectable position (e) u_{front}=-0.85, u_{back}=-2.85 the good position (f) u_{front}=-1, u_{back}=-3 the undetectable position

Fig. 15. Lying and sitting for 3 different Fresnel clearance values.

4.5 Impact of subject's respiration depth

In this section, we study the effect of respiration depth at both good and bad positions. The normal respiration frequency is around 17 times per minute while deep breath is around 6 times per minute. One cycle of variation corresponds to one inhalation and one exhalation. For lying posture, we first choose a good position ($u = 0$). We can see in Fig. 16a and 16b, both the normal and deep respiration have obvious fluctuations and clear cycles, matching the respiratory rates. For a bad position ($u = -0.85$), the deep breath has a lower respiration rate, which makes the cycle easier to be identified. However, the noise is still quite large. So deep breath is helpful for respiration detection, but it does not turn a bad position into a good position.

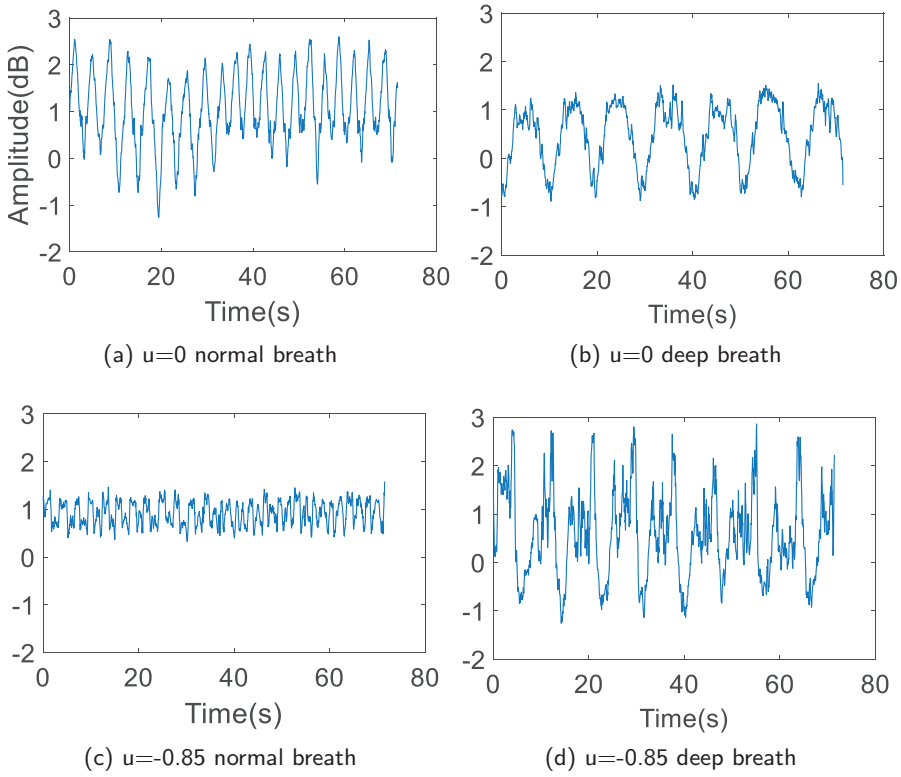

Fig. 16. Respiration depth under good and bad position.

4.6 Impact of subject's body thickness

In this group of experiments, two human subjects with different body thicknesses (i.e., 20 cm and 25 cm) lie down for respiration monitoring. As shown in Fig. 17, when the subject with a smaller body thickness is at a bad position ($u = -0.85$), the other subject is at a relatively good position ($u = -0.43$). So a bad position for person A may be a good position for person B due to the body thickness difference.

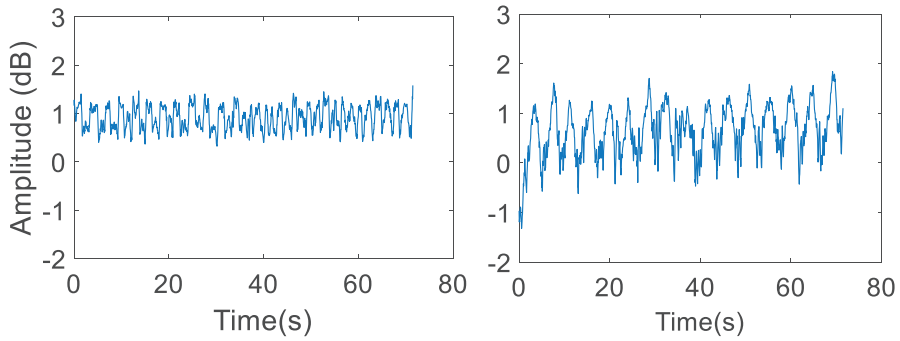

(a) Body thickness: 20 cm (b) Body thickness: 25 cm

Fig. 17. The effect of different breast thickness.

4.7 Impact of subject's distance to transceivers

Based on the analysis in Section 3.5, we carry out experiments first at a bad position ($u = 0.8$). Then we move the target to right and left by 20 cm. Fig. 18 shows the respiration-induced variations at the two positions. Compared with the result for the original position on the right, the variation slightly increases but still incurs a large amount of noise. So moving closer to one of the transceiver is not an effective way to improve the sensing capability.

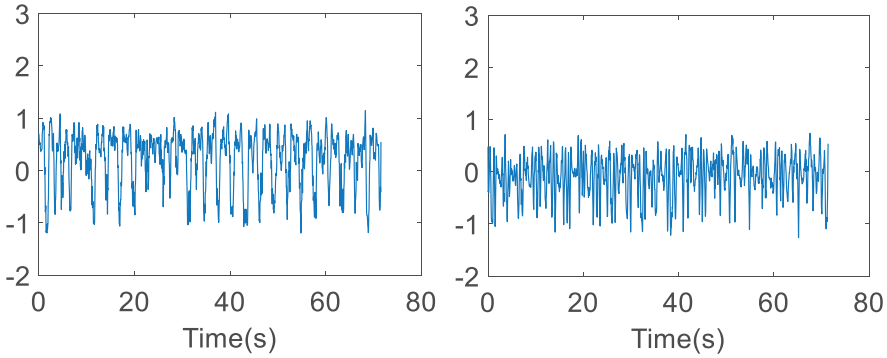

(a) d1=30 cm, d2=70 cm (b) d1=50 cm, d2=50 cm

Fig. 18. The different distance to transceivers.

4.8 Impact of subject's body orientation

Now we carry out experiments to evaluate how the system performs when the subject has different postures/orientations. For lying scenario, two more postures are considered, i.e., lying on one side and lying with face down. For sitting in the chair, three orientations are considered, i.e., parallel with LoS (0°), diagonal to LoS (45°) and perpendicular to LoS (90°).

For lying scenario, the results are shown in Fig. 19 and Fig. 20. Respiration at both postures can still be clearly detected. We observe that for lying with face down, the subject has similar back displacement as the chest displacement on the front side. The performance of respiration sensing with face down is as good as lying on the back. On the other hand, lying on one side has relatively smaller amplitude variation, because the mediolateral side of chest has smaller displacement during respiration. For sitting scenario, we observe that the clearest respiration pattern appears at 90°, and the respiration-caused variations start fading when the angle decreases towards 0°. This is due to varied chest displacements can be detected at different orientations.

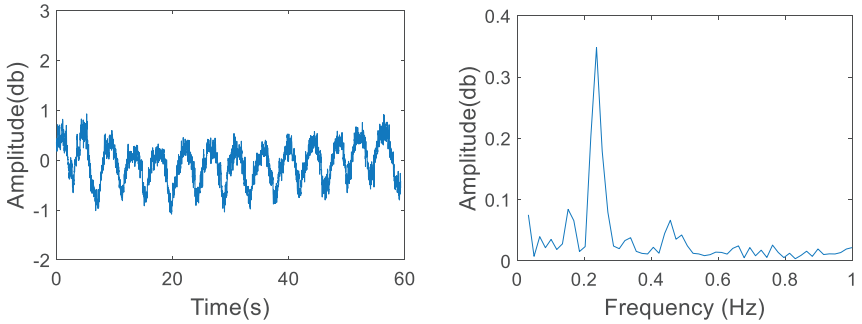

(a) Time domain (b) Frequency domain

Fig. 19. Lying on one side.

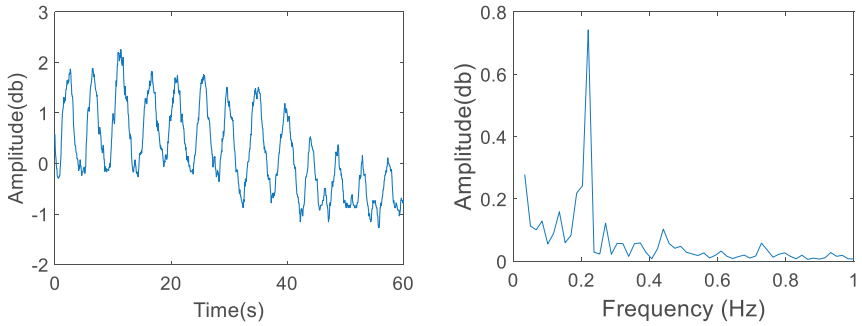

(a) Time domain (b) Frequency domain

Fig. 20. Lying with face down.

4.9 Multiple person respiration sensing

When there is more than one subject in the FFZ, the diffracted signals from multiple subjects are mixed together. When the respiration rates of multiple subjects are quite different from each other, it is still possible to obtain the respiration rate of each subject. Taking two subjects lying on the bed as

an example. The LoS distance between the transceivers is set to 1.5m. Two subjects are asked to lie side-by-side. Fig. 21a shows the amplitude variation of the signal caused by the two subjects' respirations. The respiration rates can still be distinguished in frequency domain as shown in Fig. 21b. We can see two obvious peaks, indicating the corresponding respiration rates of the two subjects, which are 8 and 18 times per minute, respectively. These results match the ground truths exactly. Note that if the two subjects have very similar respiration rates, it is still challenging for our system to obtain the accurate rates of the two subjects.

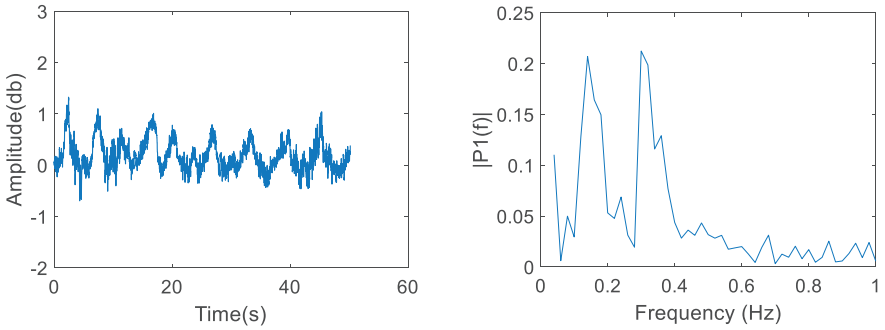

(a) Time domain (b) Frequency domain

Fig. 21. Respiration detection of Two subjects.

5 DISCUSSIONS

In this paper, we focus on utilizing the Fresnel diffraction model to guide human respiration sensing in various scenarios. We discuss several important issues related to this work below.

- ***Signal processing techniques.*** Existing work for respiration sensing utilizes various signal processing techniques (e.g., Hampel filter, Bandpass filter, etc.) to increase the accuracy. In this paper, we focus on utilizing diffraction model to explain why some locations are inherently "bad" for respiration sensing and how we can change the location just slightly to achieve a much higher accuracy. Our work is orthogonal and can be combined with the signal processing techniques to increase the amount of "good" positions among all the locations.
- ***Varying LoS distances.*** We vary the LoS distance from 1m to 2.5 m at a step size of 0.5 m and carry out experiments for both lying and sitting scenarios. We notice that the properties of Fresnel diffraction model is well preserved. When we increase the distance to 3 m and above, we find that respiration can not be reliably detected as the diffracted signal is now very weak and close to the noise level. This shows one limit of human respiration sensing with commodity Wi-Fi devices.
- ***Extending the monitoring area.*** In a smart home environment, once the target is out of the First Fresnel Zone, reflection will dominate rather than diffraction and the human respiration can be detected using our previously proposed reflection model [9]. To extend the monitoring area further, we can employ more transceiver pairs by utilizing the Wi-Fi enabled home appliances already available in the home environment. Multiple transceiver pairs will extend the monitoring area significantly.

6 RELATED WORK

Active research in wireless sensing in the last few years enables many applications ranging from coarse-grained fall detection for elderly [38] and daily activity recognition [40], to fine-grained keystroke identification [3], hand gesture recognition [13][36] and vital sign monitoring [17][16]. Most of these work leverages the signal patterns and employ pattern classification methods (e.g., SVM, C4.5) or machine learning techniques (e.g, CNN, RNN for deep learning) for matching and identification. In general, these methods need to collect a lot of activity data samples and go through a training process which is usually time-consuming and labor-intensive. Furthermore, there are usually no theoretical models or proofs provided to reveal the intuition behind the results: why these methods work, in what conditions they fail to work and what is the condition to achieve optimal results. We divide the closely related work into two categories and briefly discuss them below.

6.1 Human respiration monitoring

The research for respiration monitoring has attracted extensive attentions. There are two widely used clinical methods for monitoring respiration rate, that is, impedance pneumography [21] and capnography [4]. In smart home environments, the wearables [26] and pressure sensors [25] are adopted for long-term respiration monitoring. For the contact-free detection, cameras are used to capture the photos and image processing algorithms are applied to estimate the respiration rate. However, the camera-based methods [30] bring in severe privacy concerns and cannot be applied during night periods. Several attempts have been made using laser sensor [12] and ultrasonic sensor [10], which can measure the respiration signatures and rates in real time. Other widely used non-intrusive methods range from millimeter wave [45], sound wave [23], Doppler radar [24], UWB radar [35], FMCW radar [2][47], to Zigbee signal based methods [27][28]. However, these methods either require dedicated hardware or special-purpose devices which are not cost-effective, limiting their adoptions in home environment.

In recent years, the ubiquitous Wi-Fi signals are employed for passive human respiration sensing. These methods have clear advantages of non-intrusiveness and cost-effectiveness. Abdelnasser et al. utilizes two commodity Wi-Fi devices to extract RSS information for human respiration rate. However, the RSS readings from commodity hardware are very coarse with a low resolution. RSS readings are easily corrupted by environmental noise. In contrast, the CSI readings have richer and finer information for wireless sensing. The latest work [17][16][42][18] proposes to employ CSI readings for human respiration sensing. However, all these Wi-Fi-based methods are still based on pattern extraction and rely on advanced signal processing or machine learning techniques for identification. These methods fail to explicitly explain when and why they can achieve high accuracies. They are essentially trial-and-error based in nature.

6.2 Fresnel zone model based wireless sensing

The Fresnel diffraction model was firstly applied for device-free localization in 2015 [32] and the model was used to estimate the received signal strength (RSS) when a person with different sizes, positions and orientations is located between a pair of transceivers. The idea was further applied in [15] by utilizing the symmetry property of the diffraction effect caused by human body in a sensor network with MICAz nodes, where a subject's relative location is determined according to the RSS values. Based on the properties of Fresnel diffraction fading, the recent work [39] exploits the fact that the signal power will decrease while a person stays in the First Fresnel Zone. By using several transceivers to form multiple wireless links, it models the CSI measurements of those wireless links as a set of power fading equations, the location of the target is thus determined. However, the high density deployment of transceivers in a small area makes this method less practical in home environments. While the above work could estimate the

human's location with an accuracy of decimeter level, they did not provide a quantitative modelling for sensing the millimeter-scale human respiration in the FFZ.

The first work of human activity sensing leveraging Fresnel zone model was introduced by Wu et al. [44] and Wang et al. [9], both works deal with the case when subject is outside the FFZ. While Wu et al. [44] utilize the Fresnel reflection model to detect the human walking direction with the median error of less than 10 degrees, Wang et al. [9] apply the Fresnel reflection model for human respiration and reveal that the detectability of human respiration not only depends on the selection of subcarrier, but also one's location and orientation. Zhang et al. [46] further summarize the properties of Fresnel reflection model for human sensing with RF signals in general and derive the sensing limit of Wi-Fi signals. In their recent work, Wang et. al. [37] study the impact of static multipath on the Fresnel zone model and employ the phase difference among multiple subcarriers of the Wi-Fi signal to achieve decimeter-scale indoor localization accuracy, Wu et al. [43] classify the wireless sensing methods into two categories: machine learning-based and model-based solutions. However, the above work only studied the cases when the target stays outside the FFZ. They did not investigate the situations within the First Fresnel Zone, which is critical when the subject stays between the two transceivers.

Different from the existing work, we consider the diffraction effects for respiration sensing inside the FFZ. We employ the Fresnel diffraction model to accurately quantify the relationship between the diffraction gain and the location of the target for respiration sensing. We are the first to develop the theory and conduct experiments to clarify the distinction between lying and sitting scenarios in respiration sensing.

7 CONCLUSION

In this work, we intend to ask and answer several questions: Are there any difference for respiration sensing if a person is located at different positions in the First Fresnel Zone? Will the respiration detectability be the same for lying and sitting? Why people with different sizes at the same location might exhibit distinct sensing performance? Driven by these questions, we introduce the Fresnel diffraction model to underpin the theoretical foundation for fine-grained human respiration sensing. Comprehensive experimental results demonstrate the effectiveness of the theory we developed for respiration sensing. We believe the methodology presented in this work opens a new direction of applying radio propagation theories to study and understand wireless sensing much more deeply. Our theory can be further applied for new application with fine-grained device-free movement/activity tracking and sensing.

8 ACKNOWLEDGMENTS

This work is supported by National Key Research and Development Plan (No. 2016YFB1001200), the National Natural Science Foundation of China (No. 61472408), the Google European Doctoral Fellowship in Wireless Networking, and the Peking University Information Technology Institute (Tianjin Binhai).

REFERENCES

[1] Heba Abdelnasser, Khaled A Harras, and Moustafa Youssef. 2015. Ubibreathe: A ubiquitous non-invasive wifi-based breathing estimator. In *arXiv preprint arXiv:1505.02388 (2015)*.

[2] Fadel Adib, Hongzi Mao, Zachary Kabelac, Dina Katabi, and Robert C Miller. 2015. Smart homes that monitor breathing and heart rate. In *In Proceedings of the 33rd Annual ACM Conference on Human Factors in Computing Systems, CHI2015*. ACM, Seoul, Republic of Korea, 837–846.

[3] Kamran Ali, Alex X. Liu, Wei Wang, and Muhammad Shahzad. 2017. Recognizing Keystrokes Using WiFi Devices. *IEEE Journal on Selected Areas in Communications* 35 (2017), 1175–1190.

[4] Jay A. Anderson and Jr. William F. Vann. 1988. Respiratory monitoring during pediatric sedation: pulse oximetry and capnography. *Pediatric Dentistry* 10 (1988), 94–101.

[5] Gabriel Clavier Andre and Henri Darbord Rene. 1936. Directional radio transmission system. *Patent 2,043,347* (1936).

[6] Coleman, Westcott, and David. 2012. *Certified Wireless Network Administrator Official Study Guide*. John Wiley and Sons, Inc, 111 River St. Hoboken, NJ 07030.
[7] Francesca L. Facco, David W, Ouyang, Phyllis C. Zee, and William A. Grobman. 2014. Sleep disordered breathing in a high-risk cohort prevalence and severity across pregnancy. *American Journal of Perinatology* 31 (2014), 899–904.
[8] Daniel Halperin, Wenjun Hu, Anmol Sheth, and David Wetherall. 2011. Tool release: Gathering 802.11n traces with channel state information. *ACM SIGCOMM Computer Communication Review (CCR)* 41 (2011), 53.
[9] HaoWang, Daqing Zhang, Junyi Ma, YashaWang, YuxiangWang, DanWu, Tao Gu, and Bing Xie. 2016. Human Respiration Detection with Commodity WiFi Devices: Do User Location and Body Orientation Matter?. In *Proceedings of the International Joint Conference on Pervasive and Ubiquitous Computing, UbiComp '16*. ACM, Heidelberg, Germany, 25–36.
[10] Gregory P. Heldt and Raymond J. Ward III. 2016. Evaluation of Ultrasound-Based Sensor to Monitor Respiratory and Nonrespiratory Movement and Timing in Infants. *IEEE Transactions on Biomedical Engineering* 63 (2016).
[11] Hristo D Hristov. 2000. *Fresnel Zones in Wireless Links, Zone Plate Lenses and Antennas*. Artech House, Inc.
[12] T Kondo, T Uhlig, P Pemberton, and PD Sly. 1997. Laser monitoring of chest wall displacement. *European Respiratory Journal* 10 (1997).
[13] Hong Li, Wei Yang, Jianxin Wang, Yang Xu, and Liusheng Huang. 2016. WiFinger: talk to your smart devices with finger-grained gesture. In *Proceedings of the International Joint Conference on Pervasive and Ubiquitous Computing, UbiComp '16*. ACM, Heidelberg, Germany, 250–261.
[14] Xiang Li, Shengjie Li, Daqing Zhang, Jie Xiong, Yasha Wang, and ong Mei. 2016. Dynamic-MUSIC: accurate device-free indoor localization. In *Proceedings of the International Joint Conference on Pervasive and Ubiquitous Computing, UbiComp '16*. ACM, Heidelberg, Germany, 196–207.
[15] Chen Liu, Dingyi Fang, Zhe Yang, Hongbo Jiang, Xiaojiang Chen, Wei Wang, Tianzhang Xing, and Lin Cai. 2016. RSS Distribution-Based Passive Localization and Its Application in Sensor Networks. *IEEE Transactions on Wireless Communications* 4 (2016), 2883–2895.
[16] Jian Liu, Yan Wang, Yingying Chen, Jie Yang, Xu Chen, and Jerry Cheng. 2015. Tracking Vital Signs During Sleep Leveraging Off-the-shelf WiFi. In *In Proceedings of the 16th ACM International Symposium on Mobile Ad Hoc Networking and Computing*. ACM.
[17] Xuefeng Liu, Jiannong Cao, Shaojie Tang, and Jiaqi Wen. 2014. Wi-Sleep: Contactless sleep monitoring via WiFi signals. In *In Real-Time Systems Symposium (RTSS)*. IEEE.
[18] Xuefeng Liu, Jiannong Cao, Shaojie Tang, Jiaqi Wen, and Peng Guo. 2016. Contactless Respiration Monitoring Via Off-the-Shelf WiFi Devices. *IEEE Transactions on Mobile Computing* 15 (2016), 2466–2479.
[19] C Lowanichkiattikul, M Dhanachai, C Sitathanee, S Khachonkham, and P Khaothong. 2016. Impact of chest wall motion caused by respiration in adjuvant radiotherapy for postoperative breast cancer patients. *SpringerPlus* 5 (2016), 1–8.
[20] Se Dong Min, Jin Kwon Kim, Hang Sik Shin, Yong Hyeon Yun, Chung Keun Lee, and Myoungho Lee. 2010. Noncontact respiration rate measurement system using an ultrasonic proximity sensor. *Sensors Journal* 10 (2010), 1732–1739.
[21] Marcel Miynczak and Gerard Cybulski. 2016. Improvement of Body Posture Changes Detection During Ambulatory Respiratory Measurements Using Impedance Pneumography Signals. *Mediterranean Conference on Medical and Biological Engineering and Computing* (2016).
[22] Andreas F. Molisch. 2005. *Wireless Communications*. John Wiley and Sons, Chichester, UK.
[23] Nandakumar, Rajalakshmi, Shyamnath Gollakota, and Nathaniel Watson. 2015. Contactless sleep apnea detection on smartphones. *Proceedings of the 13th Annual International Conference on Mobile Systems, Applications, and Services* (2015).
[24] M Nowogrodzki, DD Mawhinney, and HF Milgazo. 1984. Non-invasive microwave instruments for the measurement of respiration and heart rates. *NAECON* (1984).
[25] Shoko Nukaya, Toshihiro Shino, Yosuke Kurihara, Kajiro Watanabe, and Hiroshi Tanaka. 2003. Noninvasive bed sensing of human biosignals via piezoceramic devices sandwiched between the floor and bed. *IEEE Sensors Journal* 12 (2003).
[26] Shoko Nukaya, Toshihiro Shino, Yosuke Kurihara, Kajiro Watanabe, and Hiroshi Tanaka. 2012. Noninvasive bed sensing of human biosignals via piezoceramic devices sandwiched between the floor and bed. *IEEE Sensors Journal* 12 (2012).
[27] Neal Patwari, Lara Brewer, Quinn Tate, Ossi Kaltiokallio, and Maurizio Bocca. 2014. Breathfinding: A wireless network that monitors and locates breathing in a home. *IEEE Journal of Selected Topics in Signal Processing* 8 (2014), 30–42.
[28] Neal Patwari, James Wilson, Sundaram Ananthanarayanan, Sneha Kumar Kasera, and Dwayne R Westenskow. 2014. Monitoring breathing via signal strength in wireless networks. *IEEE Transactions on Mobile Computing* 13 (2014),

1774–1786.

[29] Anders N Pedersen, Stine Korreman, Hakan Nystrom, and Lena Specht. 2004. Breathing adapted radiotherapy of breast cancer: reduction of cardiac and pulmonary doses using voluntary inspiration breath-hol. *Radiotherapy and oncology* 72 (2004), 53–60.

[30] Jochen Penne, Christian Schaller, Joachim Hornegger, and Torsten Kuwert. 2008. Robust real-time 3D respiratory motion detection using time-of-flight cameras. *International Journal of Computer Assisted Radiology and Surgery* 3 (2008), 427–431.

[31] Kun Qian, Chenshu Wu, Zimu Zhou, Yue Zheng, Zheng Yang, and Yunhao Liu. 2017. Inferring Motion Direction using Commodity Wi-Fi for Interactive Exergames. In *Proceedings of the Conference on Human Factors in Computing Systems, CHI 2017*. ACM, Denver, Colorado, USA, 1961–1972.

[32] Vittorio Rampa, Stefano Savazzi, Monica Nicoli, and Michele D'Amico. 2015. Physical Modeling and Performance Bounds for Device-free Localization Systems. *IEEE Signal Processing Letters* 22 (2015), 1864–1868.

[33] Theodore S. Rappaport. 1996. *Wireless Communications: Principles and Practices*. Englewood Cliffs, NJ, USA: Prentice-Hall.

[34] Ruth Ravichandran, Elliot Saba, Ke-Yu Chen, Mayank Goel, Sidhant Gupta, and Shwetak N Patel. 2015. WiBreathe: Estimating respiration rate using wireless signals in natural settings in the home. In *International Conference on Pervasive Computing and Communications (PerCom)*. IEEE, St. Louis, MO, USA.

[35] Svetha Venkatesh, Christopher R Anderson, Natalia V Rivera, and R Michael Buehrer. 2005. Implementation and analysis of respiration-rate estimation using impulse-based UWB. In *In Military Communications Conference, MILCOM 2005*. IEEE.

[36] Aditya Virmani and Muhammad Shahzad. 2017. Position and Orientation Agnostic Gesture Recognition Using WiFi. In *Proceedings of the International Joint Conference on Pervasive and Ubiquitous Computing, MobiSys '17*. ACM, Niagara Falls, New York, USA, 252–264.

[37] Hao Wang, Daqing Zhang, Kai Niu, Qin Lv, Yuanhuai Liu, Dan Wu, Ruiyang Gao, and Bing Xie. 2017. MFDL: A Multicarrier Fresnel Penetration Model based Device-Free Localization System leveraging Commodity Wi-Fi Cards. *arXiv cs.NI*. 50 (2017).

[38] Hao Wang, Daqing Zhang, Yasha Wang, Junyi Ma, Yuxiang Wang, and Shengjie Li. 2017. RT-Fall: A Real-Time and Contactless Fall Detection System with Commodity WiFi Devices. *IEEE Transactions on Mobile Computing* 16 (2017), 511–526.

[39] Ju Wang, Hongbo Jiang, Jie Xiong, Kyle Jamieson, Xiaojiang Chen, Dingyi Fang, and Binbin Xie. 2016. LiFS: Low Human-Effort, Device-Free Localization with Fine-Grained Subcarrier Information. In *Proceedings of the 22nd Annual International Conference on Mobile Computing and Networking, MobiCom 2016*. ACM, New York City, New York, 243–256.

[40] Wei Wang, Alex X. Liu, Muhammad Shazad, Kang Ling, and Sanglu Lu. 2017. Device-free Human Activity Recognition Using Commercial WiFi Devices. *IEEE Journal on Selected Areas in Communications* 35 (2017), 1118–1131.

[41] James C Wiltse. 1999. History and evolution of Fresnel zone plate antennas for microwaves and millimeter waves. *Antennas and Propagation Society International Symposium* 2.

[42] Chenshu Wu, Zheng Yang, Zimu Zhou, Xuefeng Liu, Yunhao Liu, and Jiannong Cao. 2015. Non-Invasive Detection of Moving and Stationary Human With WiFi. *IEEE Journal on Selected Areas in Communications* 33 (2015), 2329–2342.

[43] Dan Wu, Daqing Zhang, Chenren Xu, Hao Wang, and Xiang Li. 2017. Device-Free WiFi Human Sensing: From Pattern-Based to Model-Based Approaches. *IEEE Communications Magazine* 50 (2017), 91–97.

[44] Dan Wu, Daqing Zhang, Chenren Xu, Yasha Wang, and Hao Wang. 2016. WiDir: walking direction estimation using wireless signals. In *Proceedings of the International Joint Conference on Pervasive and Ubiquitous Computing, UbiComp '16*. ACM, Heidelberg, Germany, 351–362.

[45] Zhicheng Yang, Parth H. Pathak, Yunze Zeng, Xixi Liran, and Prasant Mohapatra. 2016. Monitoring vital signs using millimeter wave. *Proceedings of the 16th ACM International Symposium on Mobile Ad Hoc Networking and Computing* (2016), 211–220.

[46] Daqing Zhang, Hao Wang, and Dan Wu. 2017. Toward Centimeter-Scale Human Activity Sensing with Wi-Fi Signals. *IEEE Computer* 50 (2017), 48–57.

[47] Mingmin Zhao, Shichao Yue, Dina Katabi, Tommi Jaakkola, and Matt Bianchi. 2017. Learning Sleep Stages from Radio Signals: A Conditional Adversarial Architecture. In *International Conference on Machine Learning (ICML17)*. Sydney, Australia.

Received August 2017; revised November 2017; accepted January 2018